ELSEVIER

Chemical Engineering Journal 82 (2001) 231–246

Chemical Engineering Journal

www.elsevier.com/locate/cej

Comparison of CFD simulations to experiment for convective heat transfer in a gas–solid fixed bed

Michiel Nijemeisland, Anthony G. Dixon*

Department of Chemical Engineering, Worcester Polytechnic Institute, 100 Institute Road, Worcester, MA 01609, USA

Received 15 May 2000; accepted 7 October 2000

Abstract

Computational fluid dynamics (CFD) studies can improve understanding of fixed bed fluid flow and heat transfer. Our long-term objective is to use the CFD results in the development of tractable reactor models that are based on a good understanding of the fluid flow phenomena. The CFD simulations of fluid flow and heat transfer require verification to increase confidence in their use for model development. Results of a quantitative comparison between CFD results and heat transfer experimental data are given here. Simulations are presented for a model geometry of 44 solid spheres in a tube with tube-to-particle diameter ratio equal to 2. Velocity vector profiles and temperature contours have been obtained with emphasis on the wall–particle region. Comparisons are made with measured temperature profiles in a typical experimental setup with the same geometry. Several correction factors were required to compensate for non-ideal experimental measurements, and for phenomena that were not included in the CFD model. After correction, excellent agreement could be obtained between simulation and experiment.

Keywords: Computational fluid dynamics; Heat transfer mechanism; Fixed bed reactor

1. Introduction

A good qualitative understanding and an accurate quantitative description of fluid flow and heat transfer in fixed beds are important for the modeling of these devices. Accurate modeling of fixed beds is complicated, especially for tube-to-particle diameter ratio N in the range of 3–8, due to the presence of wall effects across the entire radius of the bed. With new methods such as computational fluid dynamics (CFD), it is possible to get a detailed view of the flow behavior in these beds.

Current heat transfer models for fixed bed reactors may be classified into single pseudohomogeneous phase models or two-phase heterogeneous models. Classically, these represent the fluid flow by a single, constant velocity component in the axial direction (plug-flow) with heat transfer mechanisms lumped into effective parameters. The limitations of the pseudohomogeneous approach are the subject of active research [1]; however, the heterogeneous model is more complex and requires more transport parameters to be known. For these reasons, the pseudohomogeneous model remains a popular choice for steady-state modeling. The heat transfer parameters that are needed are the effective radial thermal conductivity and the apparent wall heat transfer coefficient.

Despite over 50 years of modeling and experimental research, no consensus concerning the correlations to use to predict the effective heat transfer parameters in fixed beds has been reached. This is evident from recent papers assessing the difficulties of heat transfer or reactor modeling [2–5]. Industrial practitioners, too, find discrepancies when they try to use literature correlations from one laboratory to predict heat transfer parameters measured in another [6].

Efforts towards improvements in modeling have developed recently, and have included new approaches such as the "wave" model of dispersion and fluid flow [7,8] and the data-based Green's function methodology [9]. Many researchers have observed that the void fraction in unstructured beds is larger near the wall and fluid flow is channeled in these areas causing radial inhomogeneities in the overall flow profiles. This observation has led to the introduction of a radially varying axial velocity component $v_z(r)$ into the models to account for the presence of the wall in low-N beds. Several reactor studies have obtained better agreement with experimental data using this model [5,10–15].

It is extremely difficult to measure fluid flow inside the bed by conventional means without disturbing the packing arrangement, so the majority of studies have measured radial distributions of the axial flow outside the bed [10,16–22].

* Corresponding author. Tel.: +1-508-831-5350; fax: +1-508-831-5853.
E-mail address: agdixon@wpi.edu (A.G. Dixon).

1385-8947/01/$ – see front matter
PII: S1385-8947(00)00360-0

Nomenclature

c_p	fluid heat capacity (J/kg K)
d_p	particle diameter (m)
d_t	tube diameter (m)
G	superficial mass flow rate (kg/m^2 s)
k_f	fluid thermal conductivity (W/m K)
k_r	effective radial thermal conductivity (W/m K)
L	length of the heated bed (m)
N	tube-to-particle diameter ratio (d_t/d_p) (–)
Pe_r	radial Péclet number ($Gc_p d_p/k_r$) (–)
Pr	Prandtl number ($\mu c_p/k_f$) (–)
r	radial coordinate (m)
R	tube radius (m)
Re	Reynolds number (Gd_p/μ) (–)
T	temperature (K)
v_z	superficial axial gas velocity (m/s)
x, y	coordinates (m)
z	axial coordinate (m)

Greek symbols

ε	turbulence dissipation rate (J/s)
κ	turbulent kinetic energy (J)
μ	fluid viscosity (N s/m^2)

The earliest works found a single velocity peak, about $1d_p$–$2d_p$ from the wall. More recently, it has been observed that the flow undergoes rapid rearrangement downstream of a fixed bed [21] with the flow peaks near the wall being greatly reduced. Some studies attempted to prevent this rearrangement by using a flow splitter at the bed exit [18,23], although there is evidence that the rearrangement has already begun in the top layers of the bed [21]. Attempts have, therefore, been made to model both the velocity profiles inside the bed, and those measured downstream by use of the extended Brinkman equation [24], coupled with the Navier–Stokes equations for empty tube flow.

The desire to measure fluid flow inside the bed has led several researchers to use non-invasive experimental methods. McGreavy et al. [25,26] used laser Doppler velocimetry (LDV) in low-N packed beds for both liquid and gas experiments, although only results using liquids were presented. Stephenson and Stewart [27] used marker bubbles as a non-invasive method to measure the radial distribution of flow of a matched-refractive index fluid in transparent packed beds of equilateral cylinders with $N = 10.7$. They found that the local superficial velocity attained its global maximum at $0.2d_p$ from the wall, and its global minimum at $0.5d_p$ from the wall. Both studies found an oscillatory radial velocity profile. This type of profile was confirmed recently, again using LDV [28] for a column with a tube-to-particle diameter ratio of approximately 9. Comparisons were made with the extended Brinkman model, and good agreement was obtained if an adjustable effective viscosity was introduced into the term for wall effects. The effective viscosity depended on Re, particle shape, assumed pressure drop correlation and the wall void fraction. There is some question of whether the concept of effective viscosity should be used for packed beds [29].

The approach to packed bed modeling of including a velocity profile $v_z(r)$ in the model equations represents a modification of the earlier plug-flow approaches. It still requires the two effective heat transfer parameters to describe heat transfer, and even introduces a third effective parameter, the bed viscosity. This implies the re-correlation of these parameters using models that include the velocity profile, and the parameters will still represent several lumped transport processes [30]. Correlations for the heat transfer parameters are likely to depend on the model used for the velocity profile.

A more fundamental understanding of the fluid flow processes that effect heat transfer is required. We want to understand and include fluid behavior on the local scale. To do this, we need experimental measurements inside the bed that can identify local flow phenomena and local bed structure. Models are needed that can represent the 3D flow field and its connection to the local bed structure, and how it will influence local heat transfer rates.

A non-invasive experimental method that has been used to obtain local flow patterns in fixed beds is magnetic resonance imaging (MRI). This method can show flow patterns in complicated geometries similar to CFD modeling. The method has so far been restricted to relatively low flow rates, usually $Re < 100$, and to fluids that can produce a suitable signal for measurement, such as water. Gas flow has not been investigated by MRI techniques. Generally, the packed beds used for MRI have had a considerably higher tube-to-particle diameter ratio, which will result in less pronounced wall effects.

Qualitatively, the MRI results show generally accepted flow concepts such as flow increase in bed voids, as well as inhomogeneous velocity distribution in different pores [31,32]. The larger tube-to-particle diameter ratio also allows for a statistical view of the velocity distribution over the column cross-section. When averaged over a long evolution time, the data approached Gaussian behavior [33]. With a tube-to-particle diameter ratio of 6.7 and Re ranging from 14.9 to 44.8, the velocity profile was roughly parabolic with the maximum being near the center of the tube. Also, negative velocities or reversed flow within the bed were shown [34].

So far, there have been only a few modeling studies to try to link local fluid flow to bed structure. Chu and Ng [35] and later Thompson and Fogler [36] used network models for flow in packed beds. The different beds were established using a computer simulation method for creating a random bed. The model beds were then reduced to a network of pores, and either flow/pressure drop relations [35] or Stokes' law [36] were used to obtain a flow distribution. A very interesting approach is the use of the lattice-Boltzmann method for viscous fluid flow [37–39], that has reproduced some of

the features observed by MRI, both qualitatively and quantitatively.

The use of non-invasive experimental techniques, such as LDV and MRI, that can provide details of fluid flow inside the fixed bed, is very promising. This type of information can lead towards the development of modeling approaches that are based upon a true picture of local flow conditions in the bed. The experimental and modeling approaches to local phenomena mentioned above have so far been restricted in their application. All the experimental methods are applicable only to liquid flow, usually at low flow rates. Modeling approaches based on Stokes' law, or that neglect inertial terms, are restricted to flow rates much below those of industrial interest.

CFD is a method that is becoming more and more popular in the modeling of flow systems in many fields, including reaction engineering [40–42]. The CFD approach solves the Navier–Stokes equations and the energy balance over control volumes, small volumes within the geometry at defined locations representing the reactor internals. The results can show specific flow and heat transfer patterns that are hard to obtain with conventional modeling methods. The approach includes both laminar and turbulent flows, and is not restricted by fluid type or by flow rate.

An early study was made by Sørensen and Stewart [43,44], who computed creeping flow through packed beds, using specially designed collocation methods. They were able to obtain the velocity and temperature profiles in cubic arrays of spheres, a highly symmetric arrangement. Their calculations yielded insight into the behavior of the Nusselt number for particle heat and mass transfer, over a wide range of values of $Re\,Pr$.

Dalman et al. [45] investigated flow around two spheres near a wall using 2D finite element models in an axisymmetric radial plane. This study showed that eddies formed between the spheres, which led to regions of poor heat transfer. Lloyd and Boehm [46] also did a 2D study, with eight spheres in line, to determine the influence of the sphere spacing on the drag coefficients and the particle–fluid heat transfer coefficient. It was found that heat transfer from the spheres decreased with decreasing sphere spacing.

Three-dimensional models have been developed more recently. A simple 3-sphere model [47] focused on obtaining wall heat transfer coefficients. An 8-sphere model followed [48,49] in which the packing was modeled as two layers of four spheres. This study was limited by the absence of contact points between the spheres and the wall and between the spheres themselves.

A 10-sphere model incorporating contact points between the particles and between the particles and the wall was developed [50], which used spherical dead volumes with estimated diameters, around the contact points. The 10-sphere model showed flow behavior and heat transfer behavior that could not be described using conventional fixed bed models. Other, more recent, work in fixed beds has explored the use of CFD to simulate flow and transport in structured packings [51] and to investigate the effects of roughness gaps in particle–particle heat conduction [52].

By using CFD to thoroughly describe the local flow and heat transfer processes in a fixed bed reactor, we eventually intend to create fixed bed models based on physical processes without introducing effective, or lumped, parameters. By using the detailed flow description CFD provides, it can be determined which flow aspects can be neglected and which should be adopted in a better descriptive model.

When CFD simulations are to be used as input for modeling, it is imperative that they are checked to give viable and reliable data. In the present work, a direct comparison between CFD-generated data and experimental data is made. Heat transfer experiments have been conducted in a heated wall tube with a well-defined packing of spheres. An identical geometric model of this experimental setup has been created for CFD simulations. A series of experiments has been performed with identical boundary conditions both in the experimental setup and as a CFD simulation, and comparisons made between the two sets of results. The CFD results agreed well with the experimental data, when the same physical phenomena were present in both.

2. Experimental fixed bed description

The experimental setup used was a single packed tube with a heated wall, see Fig. 1. The packing consisted of 44 nylon–66-spheres of 25.4 mm (1 in.) diameter. The column consisted of two main parts. The bottom part was a nylon tube, 152.4 mm in length and 50.8 mm i.d., that was not directly heated, called the calming section. The purpose of the calming section was to establish a developed flow profile in the bed. The second part of the column was the heated section. It was positioned directly downstream from the calming section, and connected to it via nylon and brass flanges, using nylon bolts to reduce conduction between the sections. The double-walled heated section formed a steam jacket and was maintained at a constant temperature, heating the airflow inside the column. The 44-sphere packed bed filled the entire calming section and part of the heated section.

The wall of the column was fitted with a number of thermocouples to verify the constant heated wall temperature, as well as to establish the axial temperature profile in the calming section wall. In the double wall of the heated section, thermocouples were located at axial positions 50.8, 228.6 and 381 mm from the interface between the sections. In the calming section wall, thermocouples were installed in drilled holes at axial positions: −6.35, −15.9, −25.4, −76.2 and −127 mm from the interface between the sections. All thermocouples were type K.

Temperature measurements were taken at a series of 15 particle Reynolds numbers, and at nine different bed lengths. The temperature of the air was also measured at the column inlet. In the air stream, the radial temperature profile was measured using a thermocouple cross, inserted in the

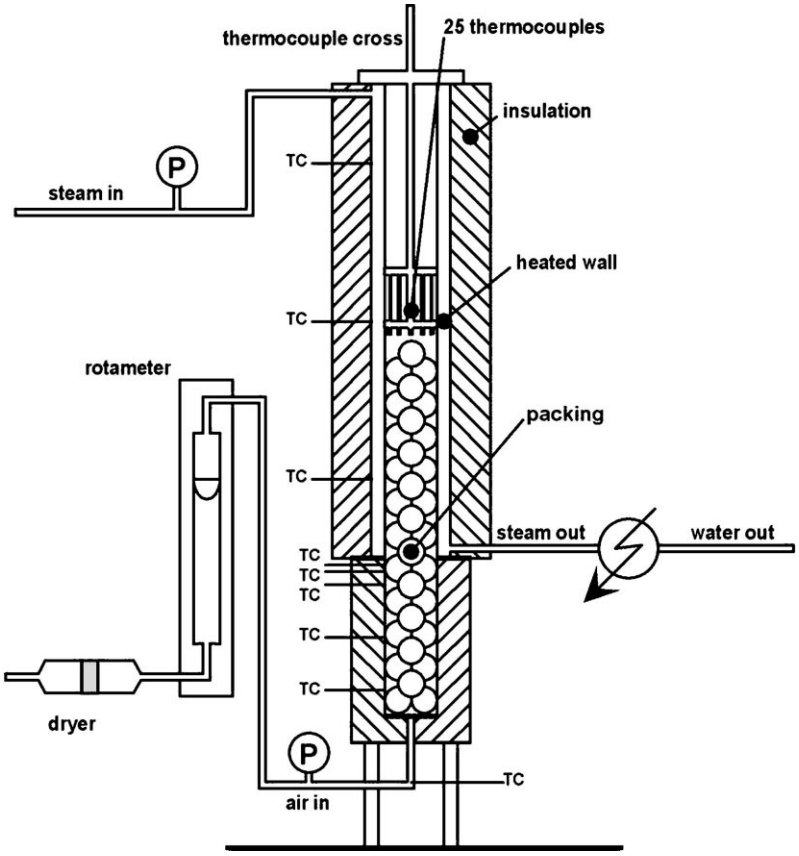

Fig. 1. The experimental setup used for the collection of temperature profiles.

column approximately 5 mm above the top layer of the bed. The cross consisted of eight arms, each holding three thermocouples. The 24 thermocouples provided four angular replicates at each of six radial positions: 7.6, 11.6, 14.2, 17.8, 20.4 and 23.2 mm from the bed centerline. The pressurized air flow through the column was drawn from an in-house system, filtered and metered by calibrated rotameters. The humidity of the pressurized air influenced the maximum flow velocity attainable, since at very humid conditions, the sudden expansion of the air within the rotameter could cause condensation.

A measurement consisted of establishing and recording a steady-state temperature profile for a combination of a specific bed length, Reynolds number and angle of thermocouple cross. A total of four thermocouple cross positions were used for measurement. Besides the initial position, measurements were taken at 15°, 30° and 45° angles from the initial orientation. By rotating the thermocouple cross, a good spread of data points covering the entire bed cross-section was ensured, giving a full picture of the angular spread of the radial temperature profile.

When all four angles had been recorded, the Reynolds number was varied by changing the flow velocity of the air through the column. A complete series consisted of 15 *Re* values ranging from the lowest possible flow at $Re = 373$ to the largest possible flow at $Re = 1922$. The upper and lower limits on *Re* were imposed by the experimental setup. The lower limit of 373 was the lowest steady flow that could be established. The upper limit of 1922 was the highest flow at which no condensation would occur.

All thermocouples were connected to a computer system for data collection. The thermocouples were connected to two Keithley Mtherm20 thermocouple boards, which read the signals from the thermocouples and connected to a Keithley Metrabus MDB64 interface unit in the computer system, where the temperature data were recorded.

For these experiments, a 44-sphere model with a tube-to-particle diameter ratio *N* of 2 was chosen. The CFD geometry had to be made identical to that of an experimental setup, so that direct comparison of data sets could be made. The packing of the spheres in the tube had to be predictable, as was the case for $N = 2$. An added advantage of this specific geometry lay in the fact that for $N = 2$, the radial heat transfer Péclet number Pe_r has similar values to these of systems with higher tube-to-particle diameter ratios [53], as shown in Fig. 2. Low-*N* systems usually have a relatively high Péclet number. As the Péclet number is the ratio of $(Re\,Pr)$ to k_r/k_f, a high Péclet number is a sign of fluid bypassing, resulting in lower k_r/k_f. Low-*N* fixed beds tend to form regular packing arrangements, allowing

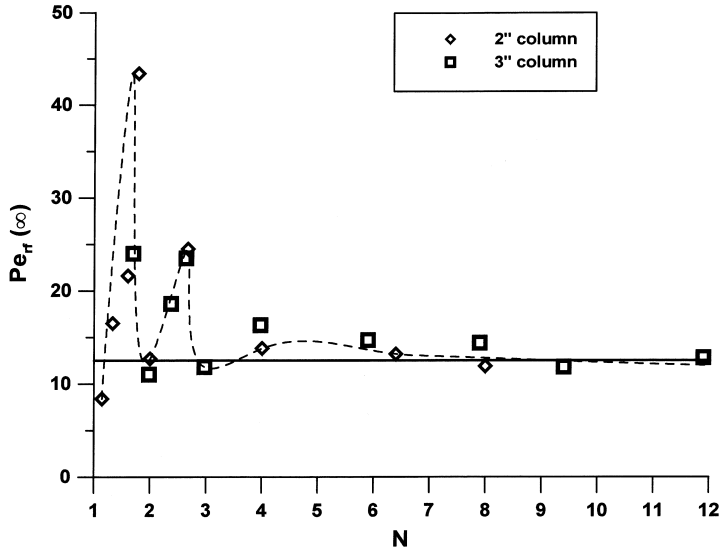

Fig. 2. Limiting fluid-phase Péclet number as a function of N for spheres.

large gaps in the packing to appear. The specific $N = 2$ system also has a regular packing structure, but the bypassing area is reduced. In the specific cases of $N = 2$ and 3, the packing is arranged in such a way that most "holes" in the packing are blocked, resulting in relatively low Pe_r and effective radial mixing. So the twofold advantage, a highly structured geometry and heat transfer properties of industrially realistic systems, made the $N = 2$ system the ideal choice for our comparison of CFD and experiment.

3. Computational fluid dynamics model

The generalized balances that are used by the Fluent commercial CFD package are the Navier–Stokes equations for conservation of mass and momentum, when it is set to calculate laminar flow without heat transfer. Additional equations are solved for heat transfer, species mixing or reaction or κ and ε for turbulent cases. The basic equations and background of these balances are stated in standard references [54].

3.1. The 44-sphere model

The CFD model is shown in Fig. 3. In this figure, the three views of the model give a better insight into its three dimensional structure. Fig. 3a shows a side view along the x-axis, giving a clear picture of the build-up of the packing. This view clearly shows the structure of the $N = 2$ packing. Fig. 3b is a top view of the model, emphasizing the tube-to-particle diameter ratio of 2 as well as the structure of this specific packing. Since the structure of the packing is so well defined, only two layers of spheres can be identified, the top view also shows how each layer of spheres blocks the bypassing created by the previous layer of spheres. Fig. 3c is a detail of the 3D mesh showing the detail of the elements in the fluid phase. It only shows the 3D mesh in the fluid region. Fig. 3 does not show the 3D mesh inside the solid particles.

Prior to the present validation study, a number of preliminary studies on CFD simulations of packed beds were done [47–50]. In the earlier studies, the mesh density was investigated extensively. From experience from these previous studies, an optimal mesh density was chosen. A short study was done to find the optimal node density, for the type of geometry used, in a limited size model. This study focused mainly on maintaining a 3D topology that described the physical model accurately and was able to handle the flow specifics of the packed bed geometry. Also, mesh densities were varied to establish the optimal mesh density, describing the flow characteristics and limiting the calculation times.

For the simulations with the 44-sphere model, the boundary conditions were set equal to the boundary conditions for the physical experiments. The outlet pressure was set at atmospheric pressure. In the experimental setup, the air outlet of the column was open to the atmosphere. The wall temperature of the heated section was set at 383 K. The wall temperature profile on the calming section required special attention, as detailed below. The air inlet temperature was set at room temperature, 298 K. The inlet velocity for each run was determined by the Reynolds number of the specific experimental run, through the definition for the Reynolds number. The initial state of all fluid elements was set to the conditions at the air inlet.

The constants in these calculations were the density of air ($1.225\,kg/m^3$), the viscosity of air ($1.7894 \times 10^{-5}\,kg/m\,s$), and the particle diameter ($2.54 \times 10^{-2}\,m$). Density and viscosity of air and therewith the Reynolds numbers were evaluated at the inlet conditions, 298 K and 1 atm. Material

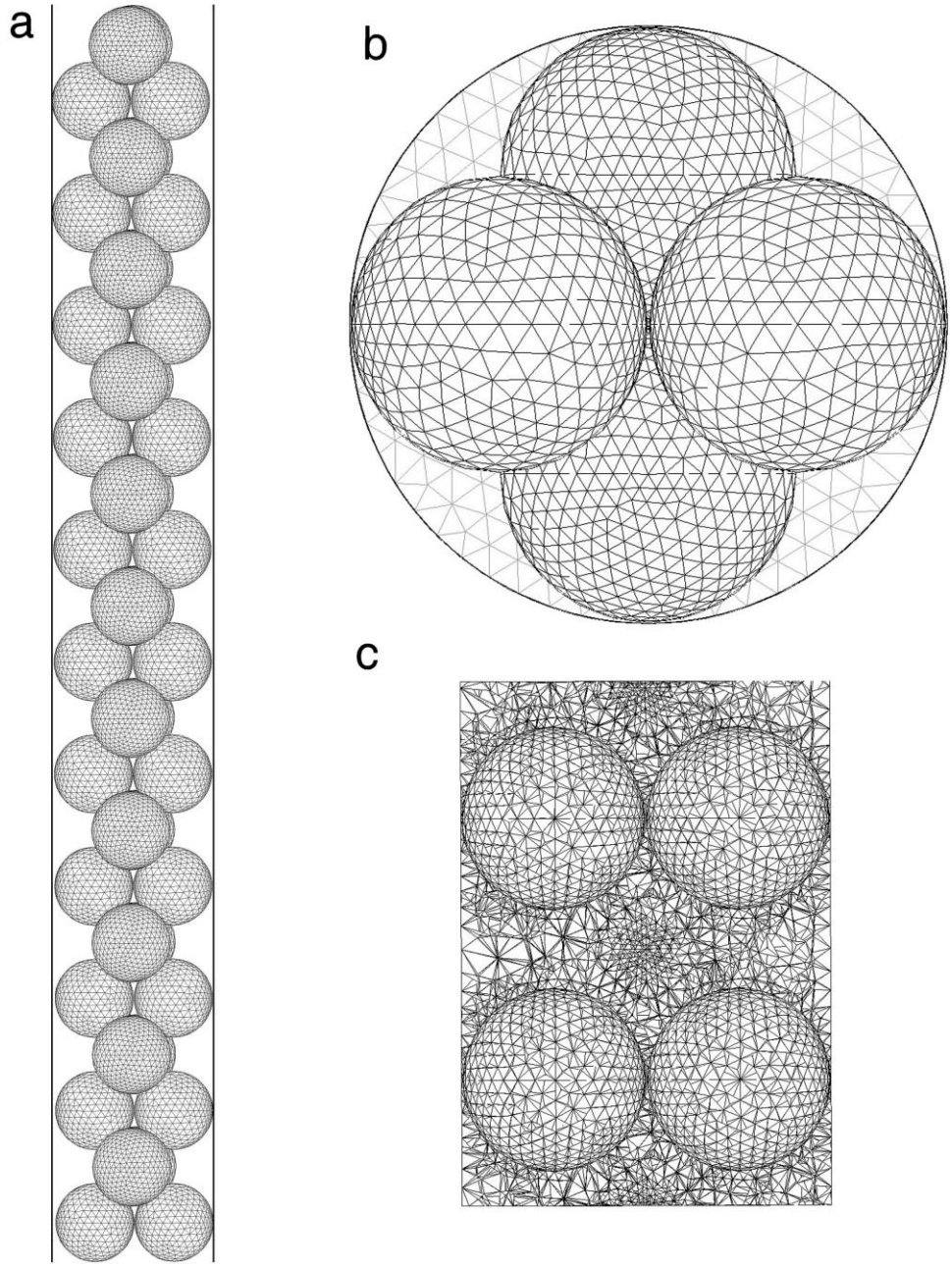

Fig. 3. CFD 44-sphere model used for validation purposes.

properties had to be defined to the program for the nylon spheres. Values were taken from work done earlier with these specific materials. A polymer was created with a density of 1300 kg/m^3, a heat capacity of 1000 J/kg K and a thermal conductivity of 0.242 W/m K [55].

3.2. Modeling contact points — the "near-miss" model

In our original CFD model, the particles and walls touched each other. The contact points between touching objects were modeled with common nodes on the surfaces of different entities. The fluid elements around these contact points then used two nodes on either wall to define their volume. When these fluid elements were created, they became very skewed, meaning that some of their surfaces were much larger than others within the one tetrahedron.

This skewed mesh around the contact points did not seem to create any problems for laminar solutions, but when a turbulent model was used to simulate the specific case convergence was unachievable. It turned out that the flow velocities, especially in the fluid elements around the contact points, were increasing dramatically, a very typical result for cells that are too skewed. In CFD, it is generally accepted that turbulent models are less stable due

to the inclusion of additional aspects, such as Reynolds stresses.

To be able to do CFD simulations at higher Reynolds numbers, which would require using a turbulent model, the model geometry had to be fundamentally changed. The fluid elements around the contact points needed to be less skewed, which could only be accomplished by creating a gap between the different entities in the geometry. This gap had to be designed carefully. Too small a gap would not eliminate the difficulties with skewed elements. Too large a gap would drastically influence the flow patterns in the system and both the convective and conductive heat transfer mechanisms. A considerable part of the conduction heat transfer into the bed occurs through a low velocity (stagnant fluid) area around the contact points.

To design the optimal gap size, several versions were created of a test model with a limited number of spheres. In each version, the spheres were created with reduced diameters, allowing for different gap sizes. The maximal sphere size that would allow for a turbulent model to be solved turned out to be 99.5% of the original sphere diameter. Other model versions were created with sphere diameters set to 99, 97 and 95% of the original. The standard for comparison was the original model, in which the spheres touched. These models were compared using histograms of the distribution of velocity magnitudes in fluid elements near the contact points, under laminar-flow conditions. The fluid elements for comparison were selected by limiting the fluid zone to an area 0.5 cm in the z and y directions from the contact point along the entire x-axis of the column (Fig. 4). In the five different geometries, air was flowed through the bed at a Reynolds number of about 20. Velocity magnitude data were taken from the different geometries and compared.

Results of the comparison are shown in Fig. 5. It may be seen that when the gaps were larger (the 95 and 97% sphere sizes), the velocity distribution tended to move to higher velocities. Both the 99.5 and 99% sphere size models showed good agreement with the touching model's velocity distribution. For further study, it was decided to use a full size 44-sphere model with 99% spheres, termed the "near-miss" model. This was chosen because this model allowed for easier construction and faster convergence than the 99.5% spheres model.

3.3. Modeling pre-heating in the calming section

When the calming section is modeled with the mathematical ideality of a CFD simulation, it can be perfectly insulated from the attached heated wall section. In the experimental setup, this insulation was not perfect, and the wall in the calming section was slightly heated through conduction. To be able to make a direct comparison between physical experiments and CFD simulations, this conduction had to be modeled, as it led to pre-heating of the gas flow in the calming section.

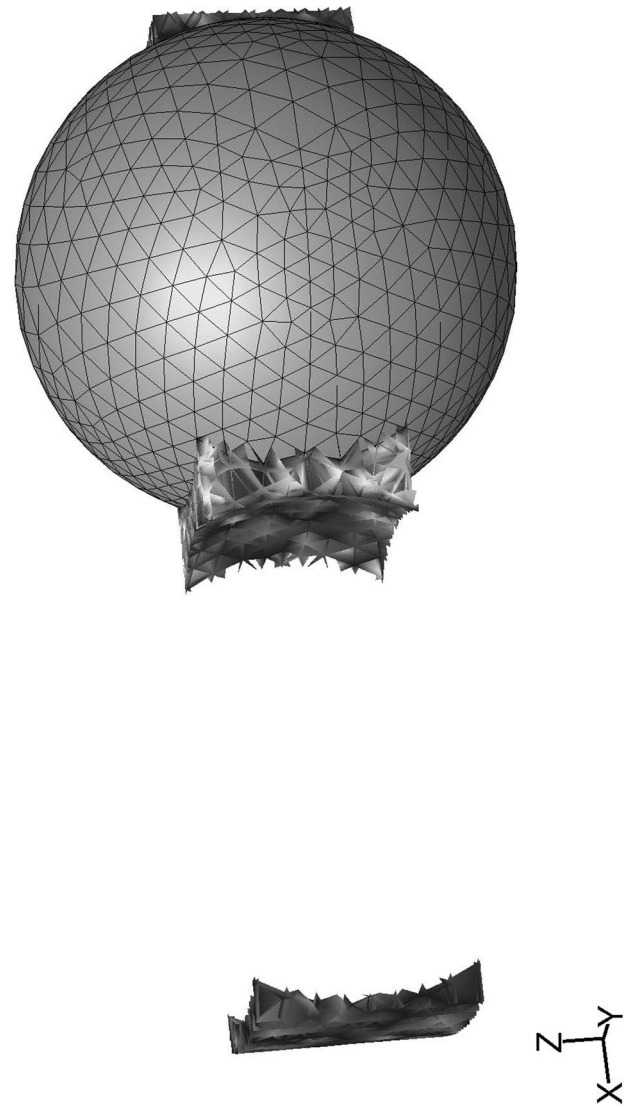

Fig. 4. Selected elements around the sphere contact points for mesh comparison.

Since the tube–wall in the model was already built up from small wall pieces, these pieces were individualized in the surface-meshing program. This process allowed different temperatures to be set for each wall segment. With the calming section wall now divided into axial sections, a model for wall conduction could be constructed.

The wall temperature profile on the calming section was determined by averaging experimentally acquired temperature data of the calming section wall over the nine separately modeled wall sections. The temperature was then implemented as a step function on the nine wall segments. The step function and experimentally measured profiles for several *Re* are shown in Fig. 6. It can be seen that axial temperature profiles in the calming section wall were only weakly dependent on *Re*, and an average temperature profile sufficed for all flow rates.

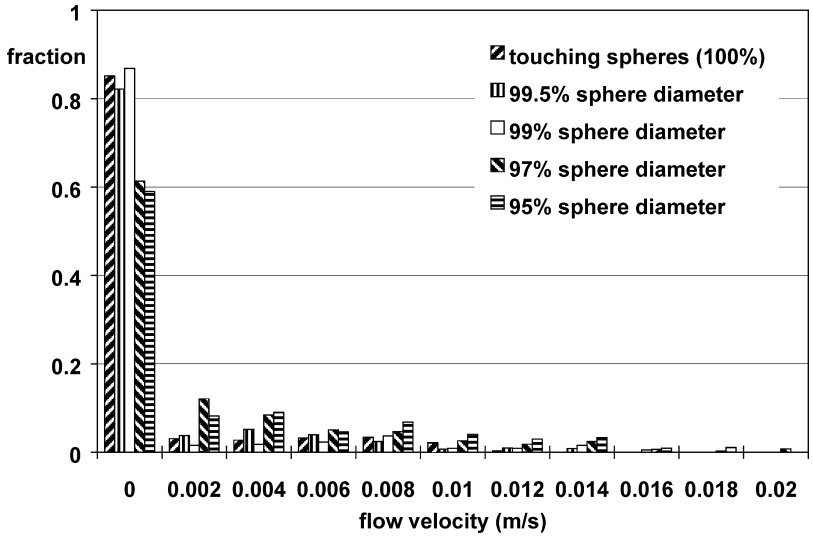

Fig. 5. Velocity histograms for comparison of the different gap sizes, $v_{in} = 0.01\,m/s$.

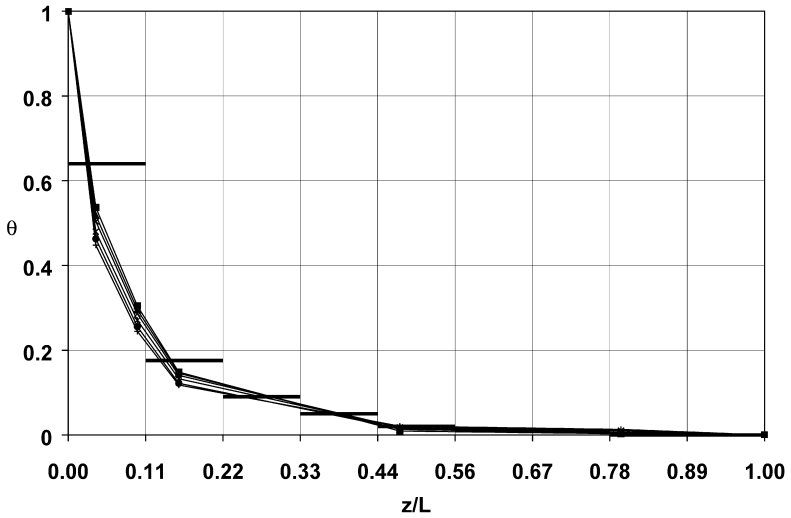

Fig. 6. Measured temperature profiles on the calming section wall at several *Re* and the step function imposed on the nine calming section wall segments.

4. Results and verification studies

The results of the CFD simulations are presented first in the form of velocity vector plots and temperature contour plots to illustrate the qualitative features and insight that can be obtained. Following the qualitative discussion, the radial temperature profiles that were extracted from the CFD data are compared quantitatively with the experimental measurements.

4.1. Qualitative features of the flow fields

A velocity vector plot is created by defining a 2D plane. The resulting data set consists of all the elements that intersect the defined plane, so that the data to be shown are not obscured by elements in front of the plane of view. Velocity vectors are displayed at the center of the projection of each element. The velocity vectors are colored according to their magnitudes, and their lengths are projections of the 3D fluid flow vectors onto the defined plane.

Fig. 7 shows a vertical section over the whole bed diameter, through the bed center, and extending two layers in the axial direction. It may be seen that the symmetric packing gives rise to a symmetric flow pattern. In this section, the areas of highest flow are in the bed center. This is because this section passes through the particle wall contacts, where the presence of the solid surfaces leads to regions of low velocity. A section at 45° to this one would pass through the open spaces next to the walls (refer to Fig. 3), where the fluid flow is at its highest. The fast flows in the middle of the bed occur as fluid squeezes its way around the particle–particle contact points. A region of circulating flow

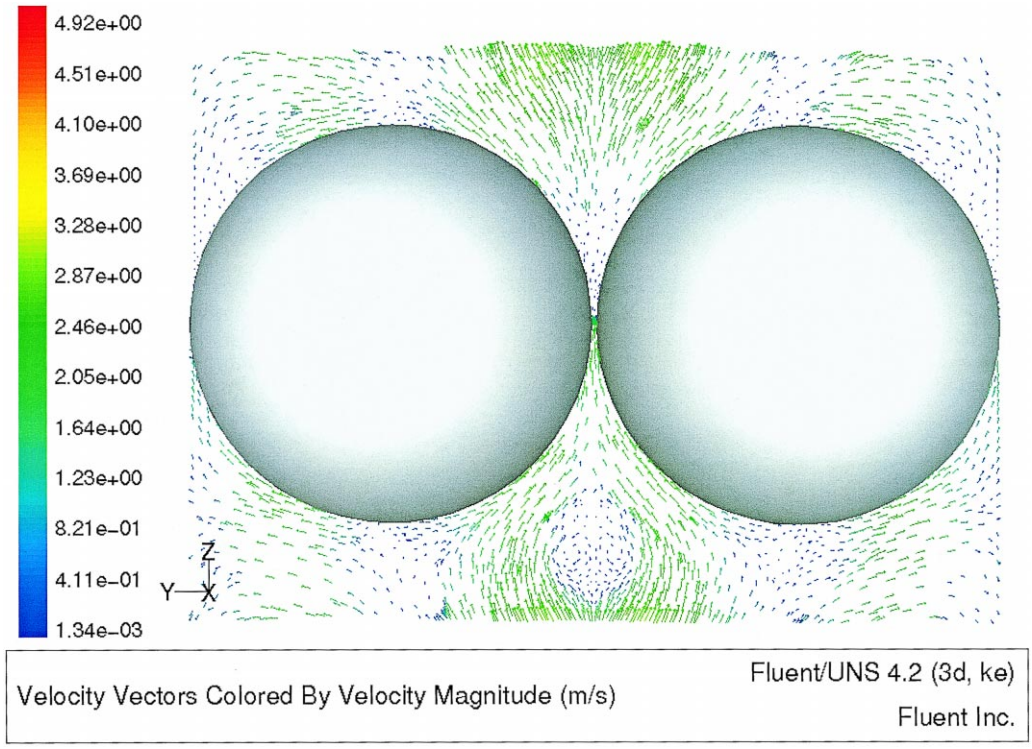

Fig. 7. Velocity vector plot for a 2-layer section over the entire bed diameter in the $x = 0$ plane at $Re = 1922$, legend shows velocity (m/s).

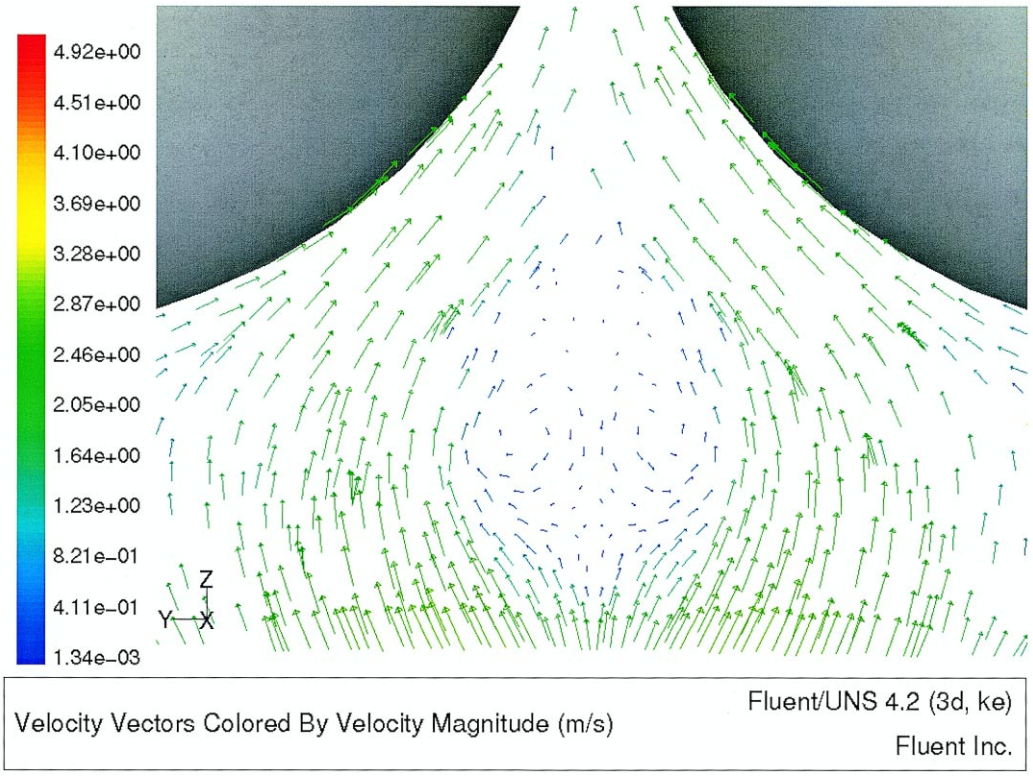

Fig. 8. Velocity vector profile at a sphere–sphere contact point, in the $x = 0$ plane at $Re = 1922$, legend shows velocity (m/s).

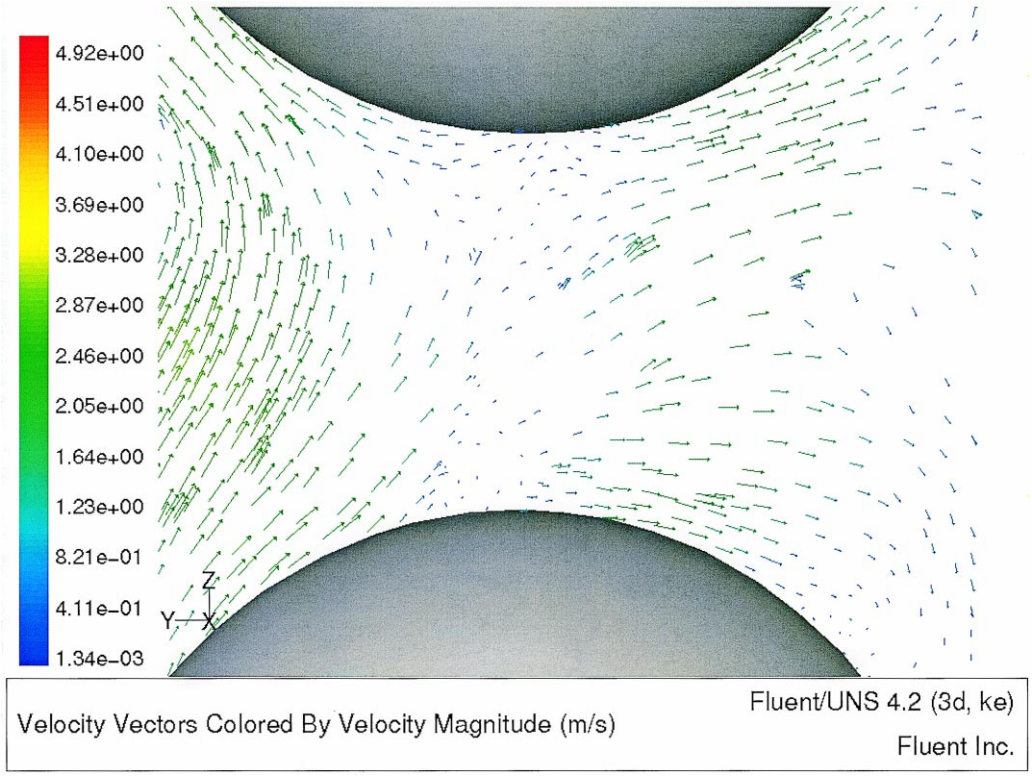

Fig. 9. Velocity vector plot in $x = 0$ plane between two sphere layers at $Re = 1922$, legend shows velocity (m/s).

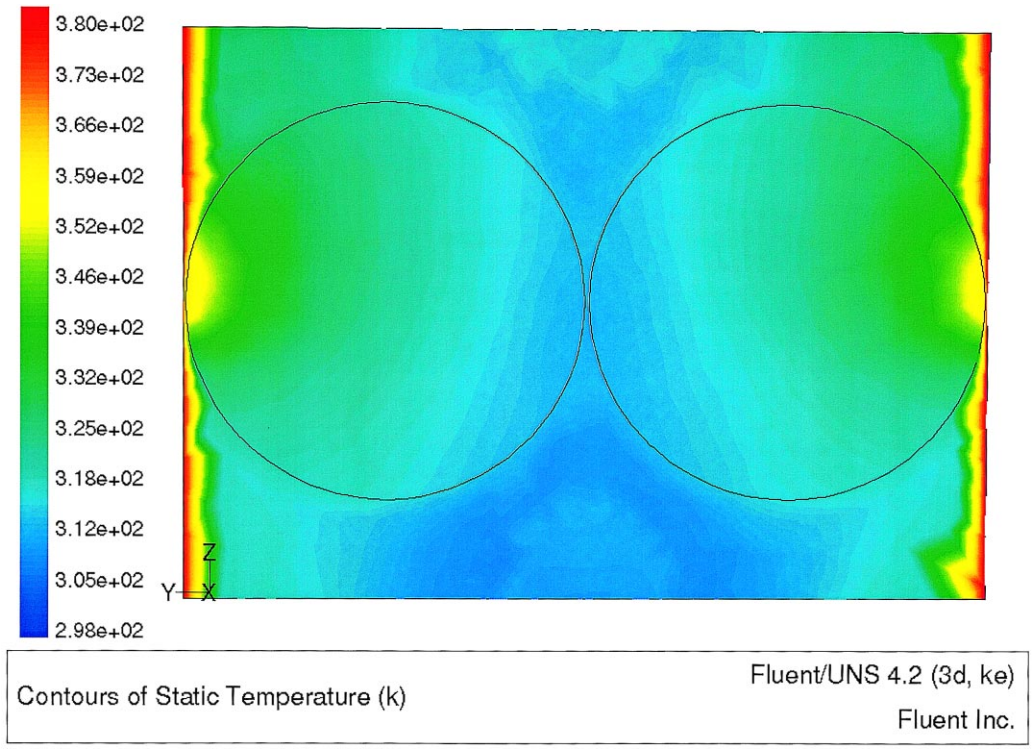

Fig. 10. Temperature contour plot for a 2-layer section over the entire bed diameter in the $x = 0$ plane at $Re = 1922$, legend shows temperature (K).

is observed around the contact point of the two spheres in the layer below the ones shown in the figure. Flow in the gap between the spheres is actually very low, the many velocity vectors that appear there are, in fact, due to the high density of elements in the gap geometry. The final feature of note is the strong radial displacements in front of and following the spheres. The efficient radial transport that these velocity components provide accounts for the good radial heat transfer in the bed that was implied by Fig. 2.

A closer look at the velocity vector field will give specific information about flow behavior near the contact points or in between layers of spheres in the bed. In Fig. 8, the contact point between the two spheres (not shown) in the layer of the packing just below the spheres shown in the top part of the picture is located near the bottom of the picture. Two important flow aspects can be identified near this sphere–sphere contact point. First, small trailing vortices form just downstream from the contact point (the overall flow direction in these pictures is from the bottom to the top). The vortices are formed in the wake of the contact point. Second, the flow magnitude in the contact point area is very low due to the close proximity to the solid particles. The flow in the small spaces is very slow, almost stagnant, confirming that stagnant fillets exist near contact points through which conduction is the main heat transport mechanism. Both these aspects are intuitive but are hard to show experimentally.

Fig. 9 shows the same plane but in a bed void instead of close to the packing. The main feature is that there is a considerable amount of radial flow. Fig. 9 ranges from the center of the column at the left-hand side of the picture to the wall at the right-hand side of the picture. Radial flow causes efficient convective heat transfer within the bed, increasing the overall heat transfer. The convective heat transfer is accomplished through transport of fluid from the center of the bed into a layer close to the wall, where most of the resistance to heat transfer occurs. Close to the wall, a local feature is visible. There is a region of relatively slow downward flow along the wall, leading to back-mixing. This last aspect of downward flow along the wall has also been shown in studies done with MRI in packed beds [34].

Fig. 10 shows temperature contours for the same section of the bed and at the same *Re* as in Fig. 7. In the center of the bed, the temperature is lower, two spherical areas can be distinguished. Below them is a region where the colder fluid drawn from upstream has accelerated past the contact point and is starting to spread out. On either wall, nearly spherical green/yellow contours show the influence of solid conduction into the particles across the wall–particle stagnant fillet. This is displaced slightly downstream from the sphere centers, due to the influence of the colder flow impinging on the upstream side of the particles. The structure of the thermal layer next to the wall is clearly seen. Upstream of the spheres, the flow moves past the sphere towards the wall, hindering heat transfer away from the wall and creating a thin layer. Downstream from the spheres, there is recirculation which enhances heat transfer to the fluid and the thermal layer is thicker. This behavior implies that the local heat transfer coefficient will vary strongly with the local flow pattern (see [48]).

4.2. Uncorrected comparisons

In this section, comparisons are made between simulated and experimental dimensionless radial temperature profiles at several different Reynolds numbers. The experimental data were collected by measuring at a particular bed length with the packing above the measurement plane removed. The CFD model was constructed to a length of 0.420 m, and radial temperature profiles obtained at that bed length with no packing above it corresponded directly to the exper-

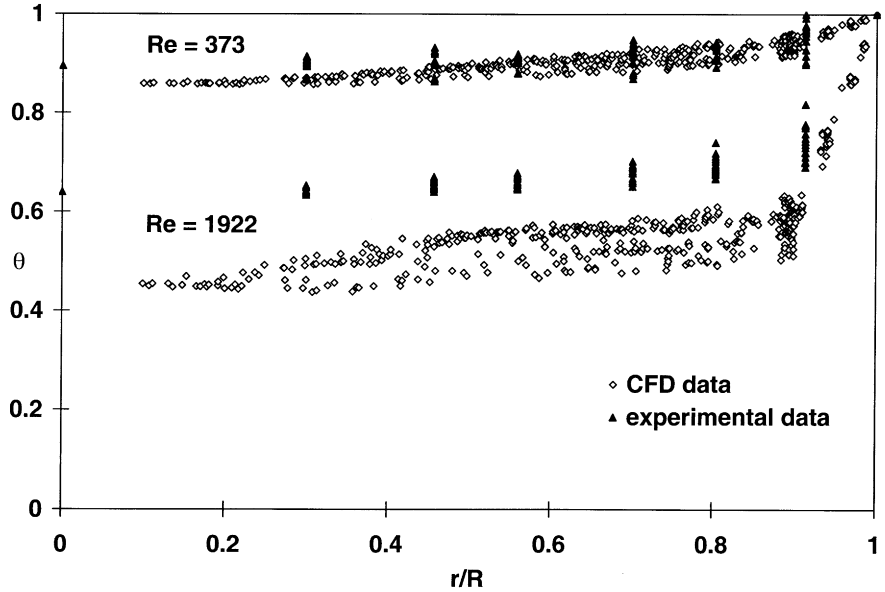

Fig. 11. Comparisons of experimental data and CFD results for the 99% near-miss model at $z = 0.420$ m.

imental situation. Unless otherwise stated, the "near-miss" model with sphere diameters at 99% of original was used for all comparisons.

Temperature profiles are shown in Fig. 11, under laminar-flow conditions at $Re = 373$ and under turbulent flow conditions at $Re = 1922$, respectively. Both sets of data showed quite flat profiles in the bed center with a very strong increase in temperature near the heated wall. This aspect was more apparent in the higher *Re* results.

The laminar-flow simulations in Fig. 11 at $Re = 373$ were also run using a model in which touching spheres were used. The "near-miss" model was also re-run under the turbulent flow option. The simulated profiles agreed to within 1 K for all three runs. For $Re = 1922$, it was also found that there was very little difference between the laminar and turbulent options.

The comparisons showed a good qualitative similarity between the CFD and experimental data. The angular variation in the experimental data at a given radial position was well reproduced by the CFD simulations, and increased from the bed center to the wall. In both cases, however, the overall temperature profile indicated by the CFD simulation was lower than for the experimental data. This difference was again more apparent at higher Reynolds numbers, and also was more pronounced in the bed center, where differences of up to 10–12 K could be found. Similar results were observed for the entire range of 15 Reynolds numbers.

4.3. Correction of systematic modeling and experimental deficiencies

In modeling using CFD, a number of assumptions are made that may each introduce a small error. Also in experimental measurements, setup limitations can introduce errors. Most of these errors individually are usually considered to be small in the overall measurements or modeling. When CFD results and experimental data are compared, however, the addition of errors can increase the overall error, leading to a misleadingly large offset between the experimental data and the CFD results. In this section, several phenomena that introduce an error in either the CFD results or the experimental measurements will be identified and discussed.

4.3.1. Experimental error due to solid conduction to the thermocouple cross

When taking experimental measurements, a thermocouple cross is lowered into the column and positioned directly above the bed. As the air flows through the bed and heats up, the thermocouples measure the gas temperature. The cross itself, however, is in contact with the heated wall and may be subject to heating through solid conduction.

To establish an estimate of the raised temperature in the thermocouple cross, an experiment was developed to measure the temperature rise in the thermocouples due to conduction alone. This implied that all heating of the thermocouples through the gas phase had to be eliminated. The thermocouple cross was installed at the lower part of the heated wall section, with the thermocouples just in the calming section, so that conduction through the nylon structure could occur without the thermocouple tips being in contact with the heated gas. To eliminate pre-heating of the gas through contact with the calming section wall, spacers were inserted between the sections, which still allowed most of the gas to flow past the thermocouple tips. This eliminated the contact area between the heated wall and the calming section wall.

Steady-state measurements were taken at two different Reynolds numbers (879, 1922) with both a heated column and a cold column. The difference between the cold and heated experiments showed the maximum heating due to conduction through the thermocouple cross. The results confirmed that the temperature measured by the thermocouple cross had been increased by conduction from the heated wall through the cross.

In this conduction experiment, heat was lost from the cross to unheated gas. At lower *Re*, this heat loss was lesser than at higher *Re*, giving higher temperature differences between the thermocouples and the gas. Under the original experimental conditions, with the cross within the heated section, the temperature in the cross would also depend on the temperature level of the gas flowing past it, which was higher at low *Re*. Thus, the driving force for conduction from the wall to the cross was less at lower *Re*, leading to lower temperature differences between thermocouples and gas at lower *Re*. This effect was eventually incorporated through a lowering of the experimental data of 2–4°C, ranging from lower to higher *Re*.

4.3.2. Contribution of radiation effects in experimental setup

Radiation effects were neglected in the CFD simulations, since it is generally accepted that radiation effects are not a factor in heat transfer processes with temperatures lower than approximately 480 K. In our setup, however, the size of the spheres is relatively large, which might make radiation a contributor to heat-up.

A calculation was done to estimate the effect of radiation. This contribution was then compared to the energy transport predicted by CFD to find if the radiation contribution was actually negligible. The CFD simulation used only conduction and convection for heat transfer into the column. An effective bed radial thermal conductivity k_{CFD} was calculated with values for flux q_{CFD} taken from the simulation. The radiation heat transfer thermal conductivity k_{RAD} was then calculated using a standard equation, which was then used to establish the radiation heat transfer flux q_{RAD}. From the augmented flux $q_{CFD} + q_{RAD}$, it was then possible to use the total thermal conductivity $k_{CFD} + k_{RAD}$ to calculate a radiation-corrected bed temperature.

For $Re = 1922$, it was found that the temperature in the CFD simulation should be approximately 2.5 K higher than

was calculated neglecting radiation. Similar calculations for $Re = 373$ showed that at this low Re, the correction to the CFD temperature was negligible, since the temperature difference between wall and particles, and hence the radiation flux, was much less.

4.3.3. Additional heat transfer through solid–wall contact points

Long-term use and production imperfections made neither the diameter of the nylon spheres nor the diameter of the tube exactly their nominal values. A number of measurements were made, and it was established that the average diameter of the spheres was slightly larger than 1 in. and the diameter of the heated section of the column was slightly smaller than 2 in. The smaller column diameter and the larger sphere diameter resulted in considerable solid–solid contact area between the wall and the spheres, resulting in extra heat transfer into the bed, which was not incorporated in the CFD model. To correct for this, the surface area was approximated and used in determining the extra heat transfer into the bed. To determine the heat transfer into the bed a modified Batchelor's equation was used [56].

Using the diameter measurements of the spheres and the column, we found an average contact radius of 1.12 mm for each sphere in the packing. A total of 28 spheres touched the heated wall with an average temperature difference between the wall and the sphere of 53 K (for $Re = 1922$). With these values, the additional heat flux into the column due to solid–solid contact between the heated wall and the packing was 1.73 W. This was about 1.3% of the heat flux into the gas phase in the CFD simulation (136 W). To correct for this additional conduction, the CFD temperatures were increased by 0.7 K, corresponding to the percentage additional heat flux into the column.

4.3.4. Modeled gap between wall and packing

It was shown from comparisons of flow profiles at several gap sizes that the small gaps used in the final model did not affect the stagnant flow area around the contact points. It did, however, make it impossible to model contact areas, as discussed above. Another aspect was an increase in conduction path length through the gas between the spheres and the wall.

A comparison of radial temperature profiles between the original model with touching spheres and the 99% near-miss model under laminar conditions, showed a lower temperature in the near-miss model, approximately 1.5 K at a Reynolds number of 373. Under turbulent conditions with no touching spheres results to compare to, one way to compare the gap influence was by directly comparing temperatures in the packing in models with different gap sizes, and extrapolating to zero gap width. The trend found in this comparison showed that for the 99% near-miss model, the temperature in the packing was approximately 2 K lower at a Reynolds number of 1922. Since the Reynolds number had little or no influence on the heat transfer through the gap, it was concluded that the flow pattern had not been significantly altered; the only influence of Reynolds number was the overall temperature difference over the column radius, the driving force for the heat transfer. The introduction of the gap caused the CFD simulations to predict too low a temperature, ranging from 1.5 K at $Re = 373$ to 2 K at $Re = 1922$.

4.3.5. Additional factors

Some other factors were investigated and found to have negligible influence on the results. These included the following:

1. In the experimental setup, a gas was fed through a small diameter inlet to the bottom of the calming section, whereas in the CFD simulation, a flat velocity profile was defined at the inlet at the bottom of the calming section. Experiments were performed with a thick layer of small nylon spheres at the bottom of the calming section inlet to disperse the flow before it reached the pre-heated calming section wall. When experimental results of the two different packing methods were compared, the difference in radial temperature profiles was only approximately 0.1°C, which fell well within the response variation of both profiles.
2. The thermocouples were re-calibrated. The calming section thermocouples were determined to have an offset up to −0.5°C; the thermocouples in the thermocouple cross were determined to have an offset up to −0.2°C. These effects counteracted each other, resulting in a negligible final temperature offset.
3. The turbulent simulations in this work were done with the standard κ–ε model. A number of runs were conducted using different turbulence models at the highest modeled Reynolds number, 1922. The additional turbulence models investigated were the renormalized group κ–ε model and the Reynolds stress model. The results of the different turbulent models were directly compared, resulting in a maximum difference of about 0.2 K. It was concluded that the different turbulence models did not show significant differences in the radial temperature profiles.

4.4. Corrected comparisons

In Table 1, a summary of the correction factors described above is given for three different Reynolds numbers. The method of calculation for the corrections was similar for all Reynolds numbers, the differences were caused mainly by changes in the temperature driving force between the wall and the center of the bed, and the difference in total energy added to the system as calculated in the CFD simulation.

Comparisons of the corrected experimental data to the corrected CFD simulations are shown in Figs. 12 and 13 for a range of Re. Fig. 12 corresponds to the uncorrected data and simulations shown previously in Fig. 11. In the corrected graphs, the experimental data and the CFD simulation are in

Table 1
Corrections on the CFD and experimental radial temperature (K) profiles

Effects	$Re = 373$		$Re = 968$		$Re = 1922$	
	CFD	Experimental	CFD	Experimental	CFD	Experimental
TC cross conduction	–	−2.0	–	−3.0	–	−4.0
Radiation	–	–	+2.1	–	+2.5	–
Solid–solid conduction	+1.6	–	+0.9	–	+0.7	–
Modeled gap	+1.5	–	+1.7	–	+2.0	–

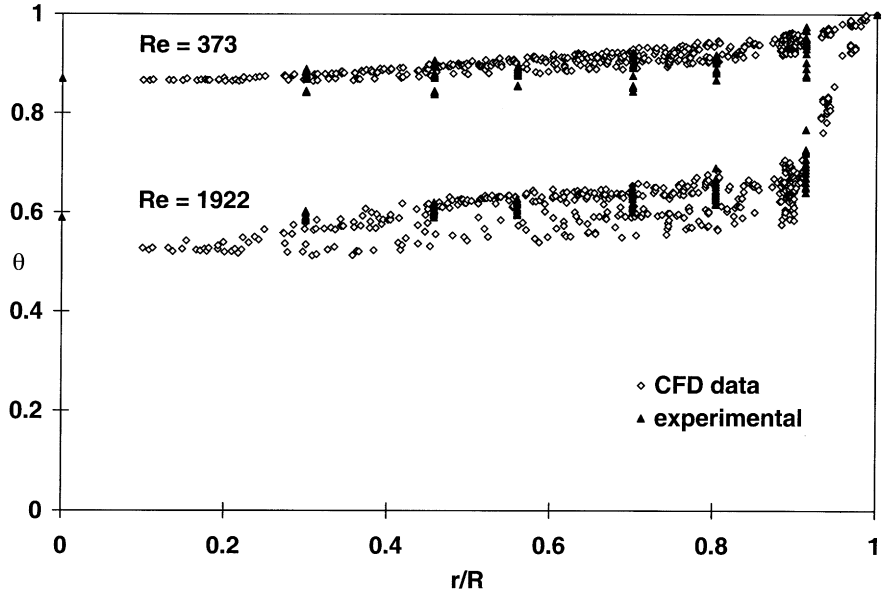

Fig. 12. Comparisons of corrected experimental and CFD results for conditions of Fig. 11 at $z = 0.420$ m.

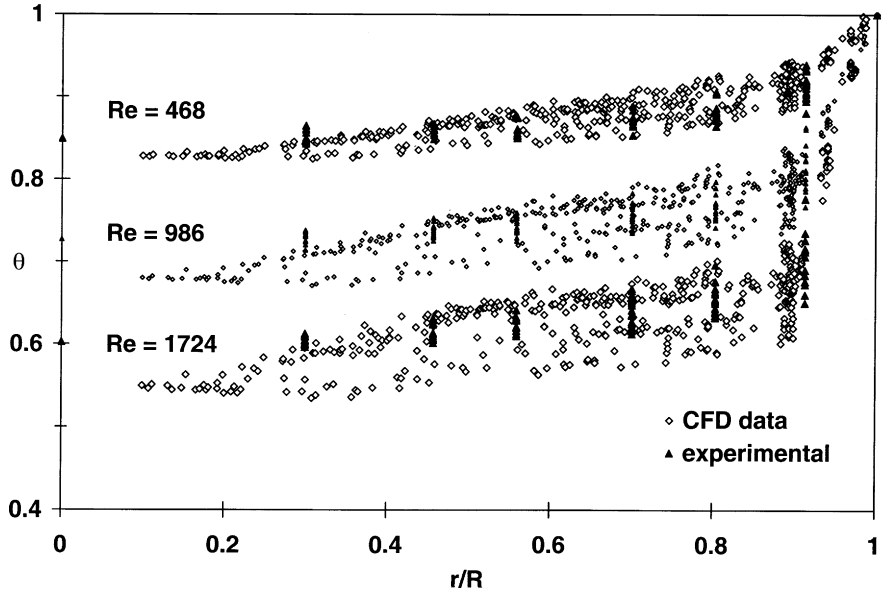

Fig. 13. Comparisons of corrected experimental and CFD results at $z = 0.420$ m.

much better agreement than they were before the correction. At the low Reynolds numbers, the largest discrepancy was found near the center of the column, in Figs. 12 and 13, the temperatures in the center of the column are in almost perfect agreement.

At higher Reynolds numbers, the discrepancy between experimental results and CFD simulations shown previously in Fig. 11 was much larger. As shown in Table 1, the correction for higher Reynolds numbers was larger as well. Figs. 12 and 13 show the corrected comparisons for several higher Reynolds numbers cases. Especially at these higher Reynolds numbers, the effects of the corrections can be seen.

It is clear that when corrections are included for both experimental and modeling deficiencies, the CFD simulations give quantitatively as well as qualitatively good agreement with the experimental results. This good agreement increases confidence that the CFD simulations may be used to provide flow information that can serve as the basis for developing more complete fixed bed reactor models.

5. Conclusions

A very good quantitative as well as an excellent qualitative fit between CFD simulation and experimental results was obtained, although this was not easily found. It was necessary to model the actual experimental setup as closely as possible, and to carefully account for any measurement biases in the experiment, as well as correcting for heat transfer mechanisms omitted from the CFD model.

Solving turbulent equations puts extra demands on a fixed bed CFD model. The distortion of the tetrahedral mesh volumes near particle–particle and particle–wall contact points presents difficulties. To be able to facilitate turbulent solution of the model, actual contact points had to be eliminated. Comparing several models with differing gap sizes between the spheres and the wall, it was found that using a sphere diameter of 99% of the actual sphere diameter allowed a turbulent solution to be obtained, as well as maintaining the original velocity distribution around the contact points.

For the case of low-N packed beds, CFD simulations are a useful tool for understanding flow and heat transfer principles, as well as for modeling these types of geometries. It is not intended to imply that the specific corrections introduced here would be applicable or necessary in all situations. Several of the corrections were specific to our particular experimental setup. For comparisons to data at other N-values, or in other equipment, different corrections may be needed. The main point is that when the comparisons are carefully done, good agreement can be achieved. A second point is that CFD simulations can give reliable information, as long as one realizes what is in the model and, more importantly, what is not.

Acknowledgements

The authors would like to thank the Fund for the Improvement of Post-Secondary Education (Department of Education) as well as the Du Pont educational fund for their financial support. Also Fluent is acknowledged for the University license of their CFD software.

References

[1] S.M.S. Dommeti, V. Balakotaiah, D.H. West, Analytical criteria for validity of pseudohomogeneous models of packed-bed catalytic reactors, Ind. Eng. Chem. Res. 38 (1999) 767–777.
[2] E. Tsotsas, E.-U. Schlünder, Heat transfer in packed beds with fluid flow: remarks on the meaning and the calculation of a heat transfer coefficient at the wall, Chem. Eng. Sci. 45 (1990) 819–837.
[3] D. Vortmeyer, E. Haidegger, Discrimination of three approaches to evaluate heat fluxes for wall-cooled fixed bed chemical reactors, Chem. Eng. Sci. 46 (1991) 2651–2660.
[4] M.G. Freiwald, W.R. Paterson, Accuracy of model predictions and reliability of experimental data for heat transfer in packed beds, Chem. Eng. Sci. 47 (1992) 1545–1560.
[5] T. Daszkowski, G. Eigenberger, A reevaluation of fluid flow, heat transfer and chemical reaction in catalyst filled tubes, Chem. Eng. Sci. 47 (1992) 2245–2250.
[6] V.G. Landon, L.A. Hebert, C.B. Adams, Heat transfer measurement for industrial packed bed tubular reactor modeling and design, AIChE Symp. Ser. 92 (1996) 134–144.
[7] W.E. Stewart, Transport phenomena in fixed-bed reactors, Chem. Eng. Prog. Symp. Ser. 61 (58) (1965) 61.
[8] A.E. Kronberg, K.R. Westerterp, Nonequilibrium effects in fixed-bed interstitial fluid dispersion, Chem. Eng. Sci. 54 (1999) 3977–3993.
[9] W.E. Stewart, D.F. Marr, T.T. Nam, A.M. Gola-Galimidi, Transport modelling of packed-tube reactors. I. Framework for a data-based approach, Chem. Eng. Sci. 46 (1991) 2905–2911.
[10] J.J. Lerou, G.F. Froment, Velocity, temperature and conversion profiles in fixed bed catalytic reactors, Chem. Eng. Sci. 32 (1977) 853–861.
[11] O. Kalthoff, D. Vortmeyer, Ignition/extinction phenomena in a wall cooled fixed bed reactor. Experiments and model calculations including radial porosity and velocity distributions, Chem. Eng. Sci. 35 (1980) 1637–1643.
[12] D. Vortmeyer, R.P. Winter, Impact of porosity and velocity distributions on the theoretical prediction of fixed-bed chemical reactor performance: comparison with experimental data, ACS Symp. Ser. 196 (1982) 49–61.
[13] H. Delmas, G.F. Froment, A simulation model accounting for structural radial non-uniformities in fixed bed reactors, Chem. Eng. Sci. 43 (1988) 2281–2287.
[14] D. Vortmeyer, P. Wagner, E. Haidegger, The interaction between temperature and flow in wall-cooled catalytic fixed-bed reactors, Chem. Eng. Sci. 47 (1992) 1325–1328.
[15] J.N. Papageorgiou, G.F. Froment, Simulation models accounting for radial voidage profiles in fixed-bed reactors, Chem. Eng. Sci. 50 (1995) 3043–3056.
[16] M. Morales, C.W. Spinn, J.M. Smith, Velocities and effective conductivities in packed beds, Ind. Eng. Chem. 43 (1951) 225–232.
[17] C.E. Schwartz, J.M. Smith, Flow distribution in packed beds, Ind. Eng. Chem. 45 (1953) 1209–1218.
[18] J. Price, The distribution of fluid velocities for randomly packed beds of spheres, Mech. Chem. Eng. Trans. 7 (1968) 14.
[19] W.W. Schertz, K.B. Bischoff, Thermal and material transport in nonisothermal packed beds, AIChE J. 15 (1969) 597–604.

[20] J. Marivoet, P. Teodoroiu, S.J. Wajc, Porosity, velocity and temperature profiles in cylindrical packed beds, Chem. Eng. Sci. 29 (1974) 1836–1840.
[21] J. Drahos, J. Cermak, I. Ziòlkowska, D. Ziòlkowski, Statistical analysis of local gas velocities at the exit from a packed bed, Chem. Eng. J. 24 (1982) 71–80.
[22] I. Ziòlkowska, D. Ziòlkowski, Modeling of gas interstitial velocity radial distribution over a cross-section of a tube packed with a granular catalyst bed, Chem. Eng. Sci. 48 (1993) 3283–3292.
[23] O. Bey, G. Eigenberger, Fluid flow through catalyst filled tubes, Chem. Eng. Sci. 52 (1997) 1365–1376.
[24] D. Vortmeyer, J. Schuster, Evaluation of steady flow profiles in rectangular and circular packed beds by a variational method, Chem. Eng. Sci. 38 (1983) 1691–1699.
[25] C. McGreavy, E.K.T. Kam, E.A. Foumeny, A. Guidoum, A.N. Ikponmwosa, A study of flow patterns in packed beds, in: Proceedings of the Second International Symposium on Application of Laser Anemometry to Fluid Mechanics, Lisbon, July 1984.
[26] C. McGreavy, E.A. Foumeny, K.H. Javed, Characterization of transport properties for fixed bed in terms of local bed structure and flow distribution, Chem. Eng. Sci. 41 (1986) 787–797.
[27] J.L. Stephenson, W.E. Stewart, Optical measurements of porosity and fluid motion in packed beds, Chem. Eng. Sci. 41 (1986) 2161–2170.
[28] M. Giese, K. Rottschäfer, D. Vortmeyer, Measured and modeled superficial flow profiles in packed beds with liquid flow, AIChE J. 44 (1998) 484–490.
[29] Subagyo, N. Standish, G.A. Brooks, A new model of velocity distribution of a single-phase fluid flowing in packed beds, Chem. Eng. Sci. 53 (1998) 1375–1385.
[30] A. Cybulski, G. Eigenberger, A. Stankiewicz, Operational and structural nonidealities in modeling and design of multitubular catalytic reactors, Ind. Eng. Chem. Res. 36 (1997) 3140–3148.
[31] A.J. Sederman, M.L. Johns, A.S. Bramley, P. Alexander, L.F. Gladden, Magnetic resonance imaging of liquid flow and pore structure within packed beds, Chem. Eng. Sci. 52 (1997) 2239–2250.
[32] A.J. Sederman, M.L. Johns, P. Alexander, L.F. Gladden, Structure-flow correlations in packed beds, Chem. Eng. Sci. 53 (1998) 2117–2128.
[33] J. Park, J.G. Gibbs, Mapping flow and dispersion in a packed column by NMR, AIChE J. 45 (1999) 655–660.
[34] Y.E. Kutsovsky, L.E. Scriven, H.T. Davis, NMR imaging of velocity profiles and velocity distribution in bead packs, Phys. Fluids 8 (1996) 863–871.
[35] C.F. Chu, K.M. Ng, Flow in packed tubes with a small tube to particle diameter ratio, AIChE J. 35 (1989) 148–158.
[36] K.E. Thompson, H.S. Fogler, Modeling flow in disordered packed beds from pore-scale fluid mechanics, AIChE J. 43 (1997) 1377–1389.
[37] J. Georgiadis, D.R. Noble, M.R. Uchanski, R.O. Buckius, Questions in fluid mechanics. Tortuous micro-flow in large disordered packed beds, ASME J. Fluid Eng. 118 (1996) 434–436.
[38] R.S. Maier, D.M. Kroll, Y.E. Kutsovsky, H.T. Davis, R.S. Bernard, Simulation of flow through bead packs using the lattice Boltzmann method, Phys. Fluids 10 (1998) 60–74.
[39] B. Manz, L.F. Gladden, P.B. Warren, Flow and dispersion in porous media: lattice-Boltzmann and NMR studies, AIChE J. 45 (1999) 1845–1854.
[40] C.K. Harris, D. Roekaerts, F.J.J. Rosendal, F.G.J. Buitendijk, Ph. Daskopoulos, A.J.N. Vreenegoor, H. Wang, Computational fluid dynamics for chemical reactor engineering, Chem. Eng. Sci. 51 (1996) 1569–1594.
[41] V.V. Ranade, Computational fluid dynamics for reactor engineering, Rev. Chem. Eng. 11 (1995) 229–289.
[42] V.V. Ranade, Improve reactors via CFD, Chem. Engr. (1997) 96–102.
[43] J.P. Sørensen, W.E. Stewart, Computation of forced convection in slow flow through ducts and packed beds. II. Velocity profiles in a simple cubic array of spheres, Chem. Eng. Sci. 29 (1974) 819–825.
[44] J.P. Sørensen, W.E. Stewart, Computation of forced convection in slow flow through ducts and packed beds. III. Heat and mass transfer in a simple cubic array of spheres, Chem. Eng. Sci. 29 (1974) 827–832.
[45] M.T. Dalman, J.H. Merkin, C. McGreavy, Fluid flow and heat transfer past two spheres in a cylindrical tube, Comp. Fluids 14 (1986) 267–281.
[46] B. Lloyd, R. Boehm, Flow and heat transfer around a linear array of spheres, Numer. Heat Trans. A 26 (1994) 237–252.
[47] O.R. Derkx, A.G. Dixon, Determination of the fixed bed wall heat transfer coefficient using computational fluid dynamics, Numer. Heat Trans. A 29 (1996) 777–794.
[48] S.A. Logtenberg, A.G. Dixon, Computational fluid dynamics studies of fixed bed heat transfer, Chem. Eng. Process. 37 (1998) 7–21.
[49] S.A. Logtenberg, A.G. Dixon, Computational fluid dynamics studies of the effects of temperature-dependent physical properties on fixed-bed heat transfer, Ind. Eng. Chem. Res. 37 (1998) 739–747.
[50] S.A. Logtenberg, M. Nijemeisland, A.G. Dixon, Computational fluid dynamics simulations of fluid flow and heat transfer at the wall–particle contact points in a fixed bed reactor, Chem. Eng. Sci. 54 (1999) 2433–2439.
[51] C. von Scala, M. Wehrli, G. Gaiser, Heat transfer measurements and simulation of KATAPAK-M catalyst supports, Chem. Eng. Sci. 54 (1999) 1375–1381.
[52] K.O. Lund, H. Nguyen, S.M. Lord, C. Thompson, Numerical correlation for thermal conduction in packed beds, Can. J. Chem. Eng. 77 (1999) 769–774.
[53] A.G. Dixon, Heat transfer in fixed beds at very low (<4) tube-to-particle diameter ratio, Ind. Eng. Chem. Res. 36 (1997) 3053–3064.
[54] S.V. Patankar, Numerical Heat Transfer and Fluid Flow, Hemisphere, Washington, DC, 1980.
[55] M.M. Melanson, Solid phase radial heat transfer in stagnant packed beds for low tube to particle diameter ratios, M.S. Thesis, Worcester Polytechnic Institute, Worcester, MA, 1984.
[56] G.J. Cheng, A.B. Yu, P. Zulli, Evaluation of effective thermal conductivity from the structure of a packed bed, Chem. Eng. Sci. 54 (1999) 4199–4209.